

Competing mechanisms of plasma transport in inhomogeneous configurations with velocity shear: the solar wind interaction with the earth magnetosphere

M. Faganello, F. Califano, F. Pegoraro
Physics Dept., University of Pisa, Pisa, Italy

Two dimensional simulations of the Kelvin-Helmholtz instability in an inhomogeneous compressible plasma with density gradient show that, in a transverse magnetic field configuration, the vortex pairing process and the Rayleigh-Taylor secondary instability compete during the non-linear evolution of the vortices. Two different regimes exist depending on the value of the density jump across the velocity shear layer. These regimes have different physical signatures that can be crucial for the interpretation of satellite data of the interaction of the solar wind with the magnetospheric plasma.

PACS numbers: 52.35.Py, 94.30.-d, 52.35.Mw, 52.65.Kj

The Kelvin-Helmholtz instability has been shown [1] to play a crucial role in the interaction between the solar wind and the Earth's magnetosphere and to provide a mechanism by which the solar wind can enter the Earth's magnetosphere. Magnetic reconnection is believed to dominate the transport properties at the low latitude magnetopause when the field in the solar wind and the geomagnetic field are antiparallel (southward solar wind magnetic field). If magnetic reconnection were the only mixing mechanism in the magnetotail, one would expect that mixing between the solar wind and the magnetospheric plasma would not occur during northward magnetic field periods. Actually, an increase of the plasma content in the outer magnetosphere during northward magnetic field periods is not only observed but is even larger than during southward configurations [1–3]. For these reasons, the Kelvin-Helmholtz (hereafter K-H) instability has been invoked as a possible mechanism in order to account for the increase of the plasma transport. In particular, the K-H instability can grow along the flank magnetopause at low latitude, where a velocity shear exists and where the nearly perpendicular magnetic field does not inhibit the development of the instability [4–6]. This provides an efficient mechanism for the formation of a mixing layer and for the entry of solar plasma into the magnetosphere, explaining the efficient transport during northward solar wind periods. Several observations support this explanation and show that the physical quantities observed along the flank magnetopause at low latitude are compatible with a K-H vortex [1, 7, 8].

Vortex pairing is believed to be the major process causing the increase in the thickness of the mixing layer in the downstream region of the magnetotail. Inverse cascade, i.e. vortex pairing, is a well known phenomenon in a two-dimensional HydroDynamic framework [9, 10], and can be expected to be an efficient process in the nearly two-dimensional external region of the magnetopause at low latitude [8, 11]. Net transport of momentum across the initial velocity shear occurs both when the Fast Growing Mode (FGM) and its sub-harmonics (paired vortices) grow, and when the vortex pairing process takes place.

In a homogeneous density system the momentum transport caused by the vortex pairing process is much larger than that due to the growth of the FGM [11] and thus leads to a faster relaxation of the velocity shear.

Several studies have focused their attention on these phenomena, providing an indirect estimate of the initial thickness of the velocity shear layer, which is not directly measured. Two different estimates were provided. The first one assumes a relationship between the period of the magnetopause oscillation in time, which increases in the downward direction along the flank magnetopause, and the size of the vortices that propagate with downstream phase velocity and at the same time undergo pairing [12, 13]. The second one is based on a direct measurement of the wave length of the vortices, taken to correspond to not yet merged FGM vortices, which is approximately eight times the initial thickness of the velocity shear layer, deduced to be $\sim 5000 - 7000$ km [1]. However, the density inhomogeneity in the layer between the solar wind and the magnetosphere strongly modifies the non-linear evolution of the K-H instability and makes the K-H vortices produce a different type of secondary instability which quickly leads to the onset of turbulence [14, 15] in the system. Indeed the centrifugal acceleration of the rotating K-H vortex acts as an "effective" gravity force on the plasma. If the density variation is large enough, the Rayleigh-Taylor (hereafter R-T) instability can grow effectively along the vortex arms. How quickly the vortex becomes turbulent is crucial since the turbulence caused by the onset of the R-T secondary instability may destroy the structure of the vortices before they coalesce and may thus be the major cause of the increase in the width of the layer with increasing velocity and density inhomogeneity. Rolled-up vortices, generated by the FGM and entering in the non-linear stage, could then evolve following an inverse cascade process [11], or by developing secondary instabilities, as for example the R-T instability [15] or Vortex Induced Reconnection (VIR) [8, 16]. The role of VIR will be discussed in a future article, since in the present letter we consider the initial magnetic field to be perpendicular to the plane where the

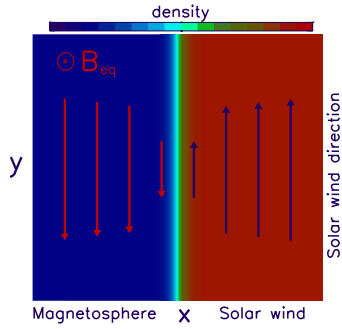


FIG. 1: Geometrical configuration adopted to describe the plasma dynamics in the equatorial plane. The arrows show the equilibrium velocity field in the comoving frame. The shading represents the equilibrium density inhomogeneity between the dense solar wind and the tenuous Magnetosphere. The equilibrium magnetic field is perpendicular to this plane.

K-H instability develops and to have no inversion points, i.e. we do not include magnetic reconnection effects. This choice allows us to isolate the processes of vortex pairing and of the development of the secondary R-T instability from processes related to VIR. We consider a 2D description of the system, with the inhomogeneity direction along x , and the y -axis along the solar wind. This choice is justified since the evolution of K-H instability is only weakly affected by slow equilibrium variation along the z -direction [5, 6]. We adopt a quasineutral plasma model described by the following set of single-fluid equations which we write in dimensionless conservative form as

$$\partial n / \partial t + \nabla \cdot (n\mathbf{U}) = 0, \quad (1)$$

with n the plasma density and \mathbf{U} the fluid velocity.

$$\partial(n\mathbf{U}) / \partial t + \nabla \cdot [n\mathbf{U}\mathbf{U} + P_T \bar{\mathbf{I}} - \mathbf{B}\mathbf{B}] = 0, \quad (2)$$

with $P_T = P + B^2/2$, which is constant at $t = 0$, and the isothermal closure

$$\partial P / \partial t + \nabla \cdot (P\mathbf{U}) = 0. \quad (3)$$

The characteristic dimensional quantities are the mass density, the Alfvén velocity and the ion skin depth. The electric field is calculated by means of Ohm's law

$$\mathbf{E} = -\mathbf{U} \times \mathbf{B}, \quad (4)$$

where electron inertia and pressure terms are neglected. The equilibrium magnetic field at $t = 0$ is taken of the form $\mathbf{B}_{eq}(x) = B_{eq}(x)\mathbf{e}_z$. In this 2D transverse configuration $\mathbf{B}(x, y, t)$ follows a pure MagnetoHydroDynamic evolution also if the Hall term is included in Ohm's law. The magnetic field contributes only to determining the degree of compressibility of the plasma in the perpendicular plane which otherwise behaves hydrodynamically.

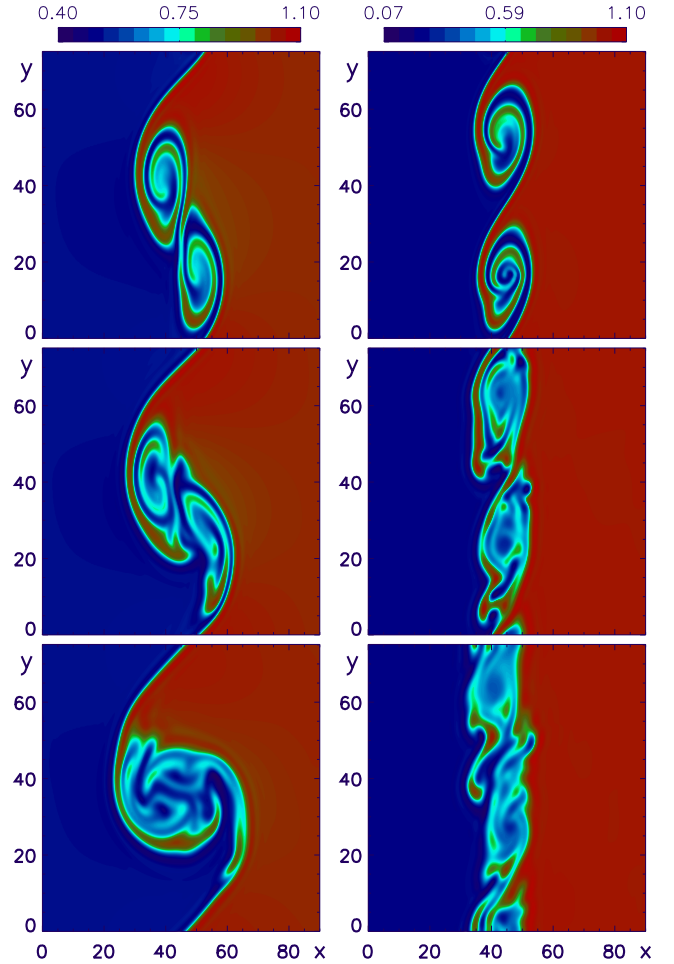


FIG. 2: Shaded isocontours in the (x, y) plane of the plasma density for an initial density jump $\Delta n = 0.5$ (first column) at $t = 370, 395, 425$ and for $\Delta n = 0.8$ (second column) at $t = 350, 392, 425$.

For the low frequency range of interest the displacement current is not included. The above equations are integrated by means of a numerical code. In this code, numerical stability is achieved by means of filters [17]. We consider an initial large-scale, sheared velocity field given by $\mathbf{U}_{eq} = (U_0/2) \tanh[(x - L_x/2)/L_u] \hat{\mathbf{y}}$ and an equilibrium density of the form $n_{eq} = 1 - (\Delta n/2) \{1 - \tanh[(x - L_x/2)/L_n]\}$. We take $L_u = L_n = 3.0$ and the box-length in the x direction $L_x = 90$. We choose the box length $L_y = 24\pi$ in the periodic y direction, in order to have well separated linear growth rates for the modes $m = 1, 2, 3$, where $m = 2$ corresponds to the FGM. The values of the two dimensionless parameters, the sound and Alfvén Mach numbers, are set as $M_s = U_0/C_s = 1.0$, $M_A = U_0/U_A = 1.0$, with $U_A = 1.0$ the value of the Alfvén velocity at $x = L_x$. First in run 1 we consider a relatively moderate initial density jump, $\Delta n = 0.5$. In Fig. 2, left column, the shaded isocontours of the plasma density show the formation and the evolution of two hy-

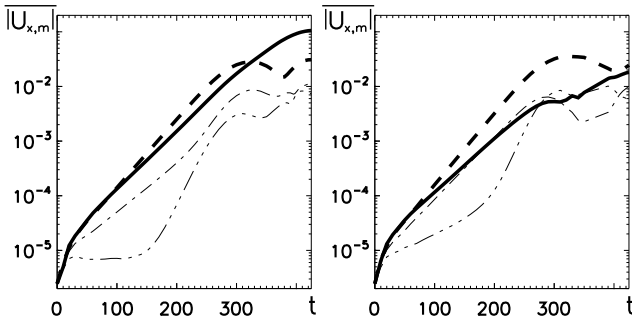


FIG. 3: Time evolution of the first four Fourier components of the plasma velocity along x , averaged along x , for an initial density jump $\Delta n = 0.5$ and for $\Delta n = 0.8$, $m=1$ continuous, $m=2$ (FGM) dashed, $m=3$ dash-dotted, $m=4$ dash - three dotted line. The $m=1$, $m=2$ lines have been drawn thicker in order to emphasize the pairing process.

hydrodynamic vortices generated by the K-H instability. We see (top frame) that two vortices, corresponding to the FGM wave number $m = 2$, start to interact (middle frame) following an inverse cascade process typical of 2D fluid systems. Eventually, the vortices merge generating a single, large scale, vortex (bottom frame). The vortex pairing process is clearly seen also in the first frame of Fig.3 where we plot the time evolution of the amplitude of the first four wave number modes of the plasma velocity field along x . In particular, the $m = 1$ mode corresponding to the largest wave length allowed in the system, initially grows at a slower rate than the $m = 2$ mode but eventually dominates for $t > 330$. In the case of a large initial density jump, $\Delta n = 0.8$, run 2, the evolution of the system is strongly affected by the development of secondary R-T instabilities inside the vortex arms as pointed out in the case of a single vortex in Ref. [15]. Indeed, see the right column of Fig.2, after the generation of the two K-H vortices, top frame, the R-T instability starts to develop inside the arms of the vortices, leading to the formation of a turbulent layer along the y -direction with typical transverse width of the order of the vortex size, bottom frame. The vortex pairing interaction is strongly depressed by the onset of the secondary instability. This is clearly shown in the right frame of Fig.3: the amplitude of the initial FGM $m = 2$ (dashed line), remains dominant even after saturation in the non-linear phase where the $m = 1$ mode (continuous line) undergoes a further increase but its amplitude remains always lower than that of the $m = 2$ mode. In order to investigate the onset of this secondary instability, we consider each of the two vortices generated by the K-H instability (right top frames of Fig.2) separately and assume such a structure to be stationary in the time interval $300 \leq t \leq 350$. During this period, the vortex propagates along the y -direction with a constant phase velocity and nearly constant amplitude. We model the vortex at $t = 300$ as an "equilibrium" configuration and

take the values n_1, u_1 and n_2, u_2 inside two nearby vortex arms connected to the more and to the less dense parts of the plasma respectively, as the density and velocity values of two superposed inhomogeneous fluid plasmas in a slab geometry. In this model, the two plasma slabs are subjected to an "effective" gravity which corresponds to the centripetal acceleration arising from the arms curvature. We label ℓ_u and ℓ_n the characteristic scale length of the velocity and density gradient between the two arms, and λ the typical wave length along the vortex arm associated to the development of the secondary instability observed in the numerical simulation. Typical (dimensionless) values are: $\ell_u \simeq \ell_n \sim 1$, $10 \geq \lambda \geq 1$.

The R-T instability is not affected by the finite value of the length ℓ_n , at least until $\lambda < \ell_n$. So, for the sake of simplicity, we can model the system by a step-like configuration. This allows us to obtain a rough estimate of the growth rate of the development of the R-T secondary instability as $\gamma_{RT} = \sqrt{\tilde{g}k(\alpha_1 - \alpha_2)}$, where $\alpha_1 = \rho_1/(\rho_1 + \rho_2)$, $\alpha_2 = \rho_2/(\rho_1 + \rho_2)$, and $\tilde{g} \simeq 0.1$ is estimated by using the value of the vortex rotation frequency and of the curvature radius of the arms. For $\lambda = 10, 4, 1$ we obtain $\gamma_{RT} \simeq 0.2, 0.3, 0.6$. On the contrary K-H modes are heavily affected by the finite value of the shear-lengths ℓ_u . According to Ref. [18], we can estimate the influence of the finite velocity shear layer on the secondary K-H instability that develops in the vortex arms, as $\gamma_{KH}^{max} \simeq 0.2 \Delta U / 2\ell_u \simeq 0.06$. Therefore, by taking into account the profiles of the velocity shear and of the density of the vortex, we conclude that the R-T instability dominates and that the estimate of its growth rate is in agreement with that observed in the numerical simulations. Furthermore we observe that the variation of the angular velocity inside the vortex is not large enough to excite the Magneto-rotational instability [19]. This suggests that this instability, which involves perturbations that depend on the ignorable coordinate z , is not important for the non-linear evolution of the KH vortex in a transverse magnetic field configuration and allows us to consider perturbations with $\partial/\partial z = 0$.

The competition between the vortex pairing process and the development of a turbulent layer driven by the onset of secondary instabilities, has important consequences from an observational point of view and can affect the transport properties of the system. In Fig.4, top left, by taking the average density value in the y direction, we observe in the pairing case a density profile inclined in the x direction with a thickness directly related to the size of the vortex which corresponds to the the $m = 2$ mode at $t = 310$ and to the the $m = 1$ at $t = 425$. In the "turbulent" case instead, (see Fig.4 top right), a "plateau" is formed in the central region of the initial sheared layer. We also note an asymmetric evolution of the average density profile, indicating a diffusion of the plasma from the dense to the tenuous region, and a typical thickness of this mixing layer comparable with

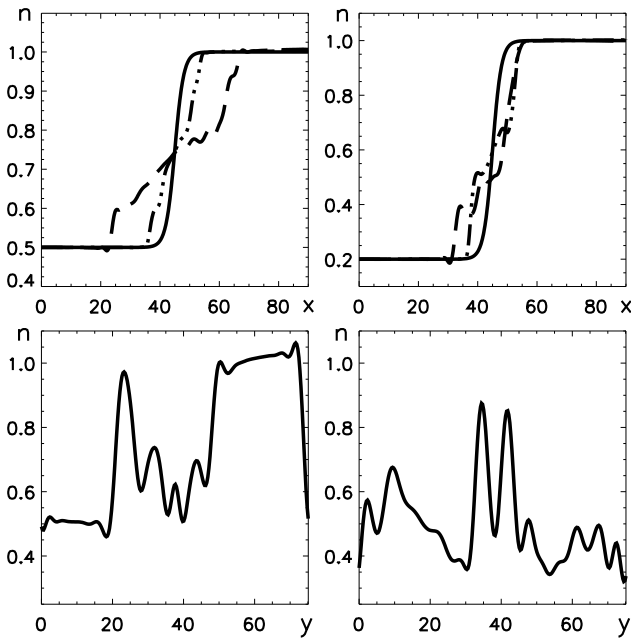


FIG. 4: Plasma average density profile along the inhomogeneity direction (first row) at $t = 0$ continuous, $t = 310$ dash - three dotted, $t = 425$ dashed line, and along the solar wind direction (second row) at $t = 425$, for an initial density jump $\Delta n = 0.5$ (first column) and for $\Delta n = 0.8$ (second column).

the FGM vortex size. In Fig.4, bottom left, we show the density profile along the y direction at $x = 45.0$ which corresponds approximately to the center of the layer. We see at $t = 425$ that the density profile is characterized by well defined structures with typical length of the order of $L_y/3$ consisting of the well known [1, 8] step-like configuration that is directly related to the two vortex arms connected to the more and to the less dense parts of the plasma, and of a filament-like configuration that is related to the more complex central region of the vortex. This profile exhibits a well-defined periodicity, given by the wave length of the vortex, and is the signature of a rolled-up vortex. It corresponds either to the FGM or to its sub-harmonics generated by the inverse cascade. On the other hand, in the case where the secondary instability develops, a sequence of alternating high and low density filaments that do not exhibit a well defined wave length is observed (see Fig.4, bottom right). This fact is related to the transition of the system to a turbulent state with the formation of a mixing layer via the development of smaller and smaller structures.

The simulations presented here show that if the R-T instability develops, it destroys the rolled-up vortices and suppresses the pairing mechanism leading to the formation of a filaments-like density profile along the solar wind direction. We think that these strong qualitative differences offer a signature that can be recognized in satellite observations and used to compare numerical data with satellite data measured along the flank magnetopause.

Since vortices propagate with downward phase velocity, increasing distance along the flank magnetopause is equivalent to time evolution in our simulations. Indeed, recently, a step-like configuration was observed in the flank magnetopause and was related to the non-linear evolution of the FGM, providing an indirect measure of the initial length scale L_u [1]. This typical signature reveals the existence of rolled-up vortices which can then evolve either following an inverse cascade process [11], or developing secondary instabilities. From an observational point of view, the long term non-linear evolution is still unclear. In measurements taken by a spacecraft further away from Earth along the solar wind direction we might expect to detect two different types of evolution. Moving downstream and following the development of the propagating vortices, we could find either step-like configurations with an increasing wave length related to the inverse cascade, or filament-like configurations that denote a rapid development to turbulence.

In conclusion the vortex pairing process and the R-T secondary instability, compete. This leads to two different regimes governed by the density jump between the solar wind and the magnetospheric plasma. When the density variation is sufficiently large, the R-T instability destroys the natural tendency of a two dimensional fluid system to self-organize its motion into coherent structures. In this case, the onset of turbulence via the secondary RT instability is an efficient mechanism of plasma transport. These two regimes have different signatures that can in principle be compared to real satellite data. This work was supported in part by PRIN-INAF 2005. We are pleased to acknowledge the “Mesocentre SIGAMM” machine, hosted by Observatoire de la Côte d’Azur, where part of the simulations was performed.

-
- [1] H. Hasegawa *et al.*, Nature **430**, 755 (2004).
 - [2] D. G. Mitchell, J. Geophys. Res. **92**, 7394 (1987).
 - [3] H. Hasegawa *et al.*, Geophys. Res. Lett. **431**, L06802 (2004).
 - [4] A. Miura, Phys. Rev. Lett. **16**, 779 (198).
 - [5] J.U. Brackbill *et al.*, Phys. Rev. Lett. **86**, 2329 (2001).
 - [6] C. Hashimoto *et al.*, Adv. Space. Res **37**, 527 (2006).
 - [7] D.H. Fairfield *et al.*, J. Geophys. Res. **105**, 21159 (2000).
 - [8] A. Otto *et al.*, J. Geophys. Res. **105**, 21175 (2000).
 - [9] C.D. Winant *et al.*, J. Fluid Mech. **63**, 237 (1974).
 - [10] F.K. Browand *et al.*, J. Fluid Mech. **76**, 127 (1976).
 - [11] A. Miura, Phys. Plasmas **4**, 2871 (1997).
 - [12] A. Miura, J. Geophys. Res. **104**, 395 (1999).
 - [13] A. Miura, Geophys. Res. Lett. **26**, 409 (1999).
 - [14] W.D. Smyth, J. Fluid Mech. **497**, 67 (2003).
 - [15] Y. Matsumoto *et al.*, Geophys. Res. Lett. **31**, 2807 (2004).
 - [16] Z.X. Liu *et al.*, Geophys. Res. Lett. **15**, 752 (1988).
 - [17] S.K. Lele, J.Comp. Phys. **103**, 16 (1992).
 - [18] A. Miura *et al.*, J. Geophys. Res. **87**, 7431 (1982).
 - [19] E.P. Velikhov, Sov. Phys. JETP **9**, 995 (1959).
 - [20] T.K.M. Nakamura *et al.*, Adv. Space. Res **37**, 522 (2006).